Detection of Left Ventricular Motion Abnormality Via Information Measures and Bayesian Filtering

Kumaradevan Punithakumar, Ismail Ben Ayed, Ian G. Ross, Ali Islam, Jaron Chong, and Shuo Li

***Abstract*—We present an original information theoretic measure of heart motion based on the Shannon's differential entropy (SDE), which allows heart wall motion abnormality detection. Based on functional images, which are subject to noise and segmentation inaccuracies, heart wall motion analysis is acknowledged as a difficult problem, and as such, incorporation of prior knowledge is crucial for improving accuracy. Given incomplete, noisy data and a dynamic model, the Kalman filter, a well-known recursive Bayesian filter, is devised in this study to the estimation of the left ventricular (LV) cavity points. However, due to similarity between the statistical information of normal and abnormal heart motions, detecting and classifying abnormality is a challenging problem, which we investigate with a global measure based on the SDE. We further derive two other possible information theoretic abnormality detection criteria, one is based on Rényi entropy and the other on Fisher information. The proposed methods analyze wall motion quantitatively by constructing distributions of the normalized radial distance estimates of the LV cavity. Using 269 $\times$ 20 segmented LV cavities of short-axis MRI obtained from 30 subjects, the experimental analysis demonstrates that the proposed SDE criterion can lead to a significant improvement over other features that are prevalent in the literature related to the LV cavity, namely, mean radial displacement and mean radial velocity.**

***Index Terms*—Cardiac wall motion abnormality, computer-aided diagnosis, information theoretic measures, level sets, MRI, recursive Bayesian filtering, Shannon's differential entropy (SDE).**

I. Introduction

CORONARY heart disease is the most common type of cardiovascular disease, and early detection of heart motion abnormality is an excellent way to diagnose and control the disease. As such, quantitative scoring of heart wall motion is of capital importance in clinical use. Due to the vast amount of information and uncertainty associated with heart motion, early detection by visual inspection is limited. Alternatively, computer-aided detection systems have attracted research attention in recent years, in order to analyze extensive amount of information associated with the heart motion. Existing methods are based on, among others, a shape parameterization for classification with principal component analysis (PCA) [1], shape models with localized variations [2], a sparse linear Fishers discriminant (SLFD) to combine several individual classifier features [3], a tensor-based classification to conserve the spatiotemporal structure of the myocardium deformation [4], a hidden Markov model (HMM) for local wall motion classification based on stress echocardiography [5], and an independent component analysis (ICA) classifier to detect and localize abnormally contracting regions [6]. In general, abnormality detection systems primarily consist of two components: preprocessing and classification.

The preprocessing component, centered around image segmentation, is in itself challenging due to the difficulties inherent to cardiac images [7]–[9]. To tackle image preprocessing, an overlap prior-based left ventricle (LV) segmentation [8], which does not require a training, is used, and the segmentation results are subsequently processed with recursive Bayesian filtering. The latter, which provides a temporal smoothing of the dataset given a suitable model, is shown to be very effective when the data is less reliable. Specifically, a cyclic model is derived in this study to characterize the dynamics of sample points of the segmented LV cavity and the Kalman filter [10] is used for state estimation. The filter estimates are subsequently analyzed to build an information theoretic classifier of heart motion.

The classification is a difficult problem due to the similarity between the statistical information associated with normal and abnormal heart motions. In this study, we investigate the problem with a global measure based on the Shannon's differential entropy (SDE). Rather than relying on elementary measurements or a fixed set of moments, the SDE measures global distribution information and, as such, has more discriminative power in classifying distributions. We further derive two other possible information theoretic abnormality detection criteria, one is based on Rényi entropy [11] and the other on Fisher information [12]. Although widely used in physics [13], computer vision [14], [15], communications [16], and many other fields, the application of information theoretic concepts is still in its early stage in medical image analysis. Few notable exceptions include using cross and joint entropy for image registration [17], [18], the Rényi entropy for measuring the heart rate Gaussianity [19], and the Shannon entropy for analyzing heart period variability [20].

Using 269 image datasets, each consisting of 20 segmented LV cavities of short-axis MR functional images, obtained from 30 subjects, the experimental analysis demonstrates that the proposed information theoretic measure of heart motion can lead

Manuscript received June 5, 2009; revised January 22, 2010; accepted May 6, 2010. Date of publication May 24, 2010; date of current version July 9, 2010. The work of K. Punithakumar was supported in part by the Natural Sciences and Engineering Research Council of Canada, under the Industrial Research and Development Fellowship.

K. Punithakumar and I. B. Ayed are with the GE Healthcare, London, ON N6A 4V2, Canada (e-mail: kumaradevan.punithakumar@ge.com; ismail.benayed@ge.com).

I. G. Ross is with the London Health Science Center, London, ON 5010, Canada (e-mail: ian.ross@lhsc.on.ca).

A. Islam is with the St. Joseph's Health Care, London, ON N6A 4V2, Canada (e-mail: ali.islam@sjhc.london.on.ca).

J. Chong is with the University of Western Ontario, London, ON N6G 1G9, Canada (e-mail: jchong2010@meds.uwo.ca).

S. Li is with the GE Healthcare, London, Ontario, N6A 4V2, Canada, and also with the University of Western Ontario, London, ON N6G 1G9, Canada (e-mail: shuo.li@ge.com).

Color versions of one or more of the figures in this paper are available online at http://ieeexplore.ieee.org.

Digital Object Identifier 10.1109/TITB.2010.2050778

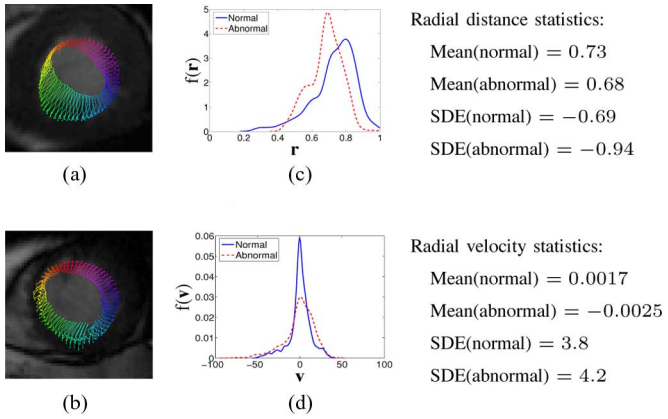

Fig. 1. Potential of the SDE measure in detecting abnormal motion. (a) Typical normal motion. (b) Typical abnormal heart. (c) and (d) Corresponding distributions of radial distances and radial velocities. A significant overlap exists between normal and abnormal motion distributions, and the corresponding first moments are approximately the same, whereas the SDEs are relatively different.

to a significant improvement over other features that are prevalent in the literature related to the LV cavity, namely, the mean radial displacement and mean radial velocity [3]. Furthermore, an analysis based on Bhattacharyya distance [21] (cf., plots in Fig. 4), which measures the separability of classes in classification problems, show that the SDE yields better classification ability amidst the stochastic nature of the cardiac motion and image segmentation inaccuracies.

The remainder of this paper is organized as follows. Section II explains the relevance of SDE for LV abnormality detection with an example. Section III describes the preprocessing of data using the level set overlap prior method. Section IV describes the temporal smoothing of data using the cyclic dynamic model and the proposed information theoretic measures. Experimental evaluations over datasets obtained from 30 subjects as well as comparisons of different classifier elements are described in Section V. Finally, the conclusions are given in Section VI.

II. Relevance of SDE for LV Motion Abnormality Detection

Fig. 1 depicts typical examples of normal and abnormal heart motion, along with the corresponding distributions of motion measurements over time. The significant overlap between these distributions makes the classification problem difficult, and the use of distribution moments, for instance, the mean [3], may not be sufficient to separate normal and abnormal motions. To tackle the classification problem, we derive an information theoretic measure of LV wall motion based on the SDE [11], which provides a *global*, theoretically grounded measure of distributions, thereby taking full advantage of the information related to cardiac motion. Rather than relying on elementary measurements or a fixed set of moments, the SDE measures global distribution information and, as such, has more discriminative power in classifying distributions. The typical examples in Fig. 1 illustrate the potential of the SDE in the classification problem: the means of abnormal and normal motion distributions are very close, whereas, the SDEs are relatively different.

III. Preprocessing of Data Using Level Set Overlap Prior

A. Tracking the Cavity Boundary

Let $\mathcal{I}$ be a MR cardiac sequence containing K frames[1] $I^k : \Omega \subset \mathbb{R}^2 \rightarrow \mathbb{R}^+$, $k \in [1, \ldots, K]$. The purpose of preprocessing is to automatically detect the boundary of the cavity of the heart (the endocardium) for each $k \in [2, \ldots, K]$. Following our work in [7] and [8], we formulate the problem as the evolution of a closed planar parametric curve $\vec{\Gamma}^k(s) : [0, 1] \rightarrow \Omega$ toward the endocardium. The curve evolution is derived from the minimization of a cost functional containing an overlap prior constraint, which prevents the papillary muscles of the cavity from being included erroneously into the heart myocardium. The papillary muscles and the myocardium are connected and have almost the same intensity profile. As such, their separation is a difficult problem [8], [9]. Assuming the cavity and myocardium regions in the first frame I^1, denoted by C^1 and M, respectively, are given, for instance, using a user initialization, the problem consists of segmenting domain Ω of each frame k, $k \in [2, \ldots, K]$, into two target regions: 1) the heart cavity C^k corresponding to the interior of curve $\vec{\Gamma}^k$, denoted $C^k = \mathbf{R}_{\vec{\Gamma}^k}$, where $\mathbf{R}_{\vec{\Gamma}}$ is the region $\vec{\Gamma}$ encloses, and 2) the background B^k corresponding to the region outside $\vec{\Gamma}^k$, $B^k = \mathbf{R}^c_{\vec{\Gamma}^k}$, where superscript c indicates complement. The evolution equation of $\vec{\Gamma}^k$ is obtained by gradient-descent minimization of a cost functional containing three characteristic terms [7], [8] as given in

$$\begin{aligned} \mathcal{F}^k = & \underbrace{\alpha(\mathbf{B}^k - \mathbf{B}^1)^2}_{\text{cavity/myocardium overlap prior}} \\ & + \underbrace{\beta(\mu^k - \mu^1)^2}_{\text{Cavity mean matching}} \\ & + \underbrace{\lambda \oint_{\vec{\Gamma}^n} (g_k + c) ds}_{\text{Edge detection and smoothing}} \end{aligned} \tag{1}$$

where $\mathbf{B}^k$ is the Bhattacharyya coefficient measuring the amount of overlap between the intensity distribution within the heart cavity in I^k and the myocardium model distribution learned *a priori* from the first frame, μ^k is the estimate of intensity mean within C^k, g_k is an edge indicator function, and c is a positive constant. α, β, and λ are positive constants weighing the contribution of each term. The expressions of $\mathbf{B}^k$, μ^k, and g_k are given in the Appendix A. The first term measures the conformity of the overlap between the intensity distribution within the cavity in current frame k and the myocardium model to prior information on such overlap $\mathbf{B}^1$ learned from the first frame. The second term measures the conformity of intensity mean within the cavity in current frame k to a mean prior learned from the first frame. The last term biases the active curve toward high gradient of intensity and enforces curve smoothness. Since tracking the cavity is not the focus of this study, we refer the readers to [8] for further details on the curve evolution equation

[1]Number of frames K is typically equal to 20 or 25.

minimizing this functional, the corresponding computation and implementation details, and further discussion on the relevance of the functional to cardiac cavity tracking. It is worth noting that other tracking algorithms can be used as a preprocessing step.

IV. Method

A. Temporal Smoothing

1) Dynamic Model for Temporal Periodicity: Let $(\mathrm{x},\ \mathrm{y})$ be a Cartesian point on the endocardial boundary $\vec{\Gamma}^k(s)$ obtained from the preprocessing described earlier. Consider the state vector $\xi = [\bar{\mathrm{x}}\ \mathrm{x}\ \dot{\mathrm{x}}]^T$ that describes the dynamics of the point in x-coordinate direction, where $\dot{\mathrm{x}}$ and $\bar{\mathrm{x}}$ denote velocity and the mean position over a cardiac cycle, respectively. We assume the heart motion is periodic. A *continuous state-space* model that describes the cyclic motion of the point is given by

$$= A(t)\xi(t) + Bw(t) \tag{2}$$

where

$$A(t) = \begin{bmatrix} 0 & 0 & 0 \\ 0 & 0 & 1 \\ \omega^2 & -\omega^2 & 0 \end{bmatrix}, B = \begin{bmatrix} 1 & 0 \\ 0 & 0 \\ 0 & 1 \end{bmatrix},$$

ω is the angular frequency, and $w(t)$ is the white noise that accounts for approximating the unpredictable modeling errors arising in LV motion. Model (2) is linear for a given ω and can be viewed as an approximation of the temporal periodic model used in [22], where higher order terms of the Fourier expansion were neglected. The *discrete-time equivalent*[2] of (2) can be derived as follows (refer to Appendix B for derivation details):

$$\xi_{k+1} = F_{cy}(k)\xi_k + w_k \tag{3}$$

where

$$F_{cy}(k) = \begin{bmatrix} 1 & 0 & 0 \\ 1-\cos(\omega T) & \cos(\omega T) & \dfrac{1}{\omega}\sin(\omega T) \\ \omega\sin(\omega T) & -\omega\sin(\omega T) & \cos(\omega T) \end{bmatrix}.$$

The covariance of process noise $Q_k = \mathrm{cov}(w_k)$ is given by

$$Q_k = [q_{ij}]_{3\times 3} \tag{4}$$

where q_{ij}'s are defined in (56)–(61) in Appendix B. We can consider the state vector $\mathbf{s} = [\bar{\mathrm{x}}\ \mathrm{x}\ \dot{\mathrm{x}}\ \bar{\mathrm{y}}\ \mathrm{y}\ \dot{\mathrm{y}}]^T$ that describes the dynamics in x–y plane. The discrete state-space model in x–y plane is given by

$$\mathbf{s}_{k+1} = \begin{bmatrix} F_{cy}(k) & \mathbf{0}_{3\times 3} \\ \mathbf{0}_{3\times 3} & F_{cy}(k) \end{bmatrix}\mathbf{s}_k + v_k = F_k\mathbf{s}_k + v_k. \tag{5}$$

2) Recursive Bayesian Filtering: Kalman filter, which yields an optimal estimate for linear/Gaussian systems, is applied for state estimation. Let $z_k = [z_{k,\mathrm{x}}\ z_{k,\mathrm{y}}]^T$ be the measurement at time step $k \in [1,\ldots,K]$. Then, the measurement equation is given by

$$z_k = H_k\mathbf{s}_k + \eta_k \tag{6}$$

where

$$H_k = \begin{bmatrix} 0 & 1 & 0 & 0 & 0 & 0 \\ 0 & 0 & 0 & 0 & 1 & 0 \end{bmatrix} \tag{7}$$

and η_k is a zero-mean Gaussian noise sequence with covariance

$$R_k = \begin{bmatrix} r & 0 \\ 0 & r \end{bmatrix}. \tag{8}$$

One cycle recursion of the Kalman filter is summarized as follows.

a) Kalman Filter Prediction: The *predicted state* is obtained by following state equation (5) and taking the expectation conditioned on $z_{1:k} = \{z_1,\ldots,z_k\}$. Let $\mathbf{m}_k = \mathbb{E}[\mathbf{s}_k]$ be the mean of the state vector. The state-prediction equation is given by

$$\mathbf{m}_{k+1}^- = F_k\mathbf{m}_k. \tag{9}$$

The corresponding *state-prediction covariance* is given by

$$P_{k+1}^- = F_kP_kF_k^T + Q_k. \tag{10}$$

b) Kalman Filter Update: The *measurement residual* or *innovation* follows by taking the expectation conditioned on $z_{1:k}$:

$$\nu_{k+1} = z_k - H_k\mathbf{m}_{k+1}^- \tag{11}$$

whereas the corresponding *innovation covariance* is given by

$$S_{k+1} = H_kP_{k+1}^-H_k^T + R_k \tag{12}$$

and the filter gain is computed as follows:

$$W_{k+1} = P_{k+1}^-S_{k+1}^{-1}. \tag{13}$$

Then, the *updated-state estimate* can be calculated as follows:

$$\mathbf{m}_{k+1} = \mathbf{m}_{k+1}^- + W_{k+1}\nu_{k+1}. \tag{14}$$

Finally, the *updated-state covariance* is given by

$$P_{k+1} = P_{k+1}^- - W_{k+1}S_{k+1}W_{k+1}^T. \tag{15}$$

c) Filter Initialization: In our problem, we do not have *prior* knowledge of the initial value of $\mathbf{s}_1$. Therefore, we use *two-point differencing* method [10] to initialize position and velocity components of the state. For instance, the initial position and velocity elements in x-coordinate direction are given by

$$\hat{\mathrm{x}}_1 = z_{1,\mathrm{x}} \tag{16}$$

$$\hat{\dot{\mathrm{x}}}_1 = \frac{(z_{2,\mathrm{x}} - z_{1,\mathrm{x}})}{T}. \tag{17}$$

The mean position over cardiac cycle $\bar{\mathrm{x}}$ is initialized by taking the expectation over all corresponding measurements

$$\hat{\bar{\mathrm{x}}}_1 = \frac{1}{K}\sum_{k=1}^{K} z_{k,\mathrm{x}}. \tag{18}$$

The initial-state elements in y-coordinate direction $\hat{\mathrm{y}}_1$, $\hat{\dot{\mathrm{y}}}_1$, and $\hat{\bar{\mathrm{y}}}_1$, can be computed similarly using $\{z_{k,\mathrm{y}}\}$. The corresponding initial covariance is given by

$$P_1 = \begin{bmatrix} \Phi_1 & \mathbf{0}_{3\times 3} \\ \mathbf{0}_{3\times 3} & \Phi_1 \end{bmatrix} \tag{19}$$

[2]Term discrete-time equivalent refers to the model if the discretization is exact and the continuous and discrete-time process noises have equivalent effects, which varies from direct discrete-time models known as discrete-time counterparts [23].

where

$$\Phi_1 = \begin{bmatrix} r & \frac{r}{K} & \frac{r}{KT} \\ \frac{r}{K} & r & \frac{r}{T} \\ \frac{r}{KT} & \frac{r}{T} & \frac{2r}{T^2} \end{bmatrix}. \tag{20}$$

In some very rare cases, the segmentation results of the LV are not consistent over a cardiac cycle. We detect such inconsistencies by gating the center of the segmented LV. Let $\{\mathbf{s}_k^i = [\bar{\mathsf{x}}_k^i \;\; \mathsf{x}_k^i \;\; \dot{\mathsf{x}}_k^i \;\; \bar{\mathsf{y}}_k^i \;\; \mathsf{y}_k^i \;\; \dot{\mathsf{y}}_k^i]^T : i = 1, \ldots, N\}$ be a sample point in the LV boundary in frame k. We define the center of the LV cavity $(c_{\mathsf{x},k} \;\; c_{y,k})$ by

$$\begin{cases} c_{\mathsf{x},k} = \dfrac{1}{N}\displaystyle\sum_{i=1}^{N} \mathsf{x}_k^i \\ c_{\mathsf{y},k} = \dfrac{1}{N}\displaystyle\sum_{i=1}^{N} \mathsf{y}_k^i. \end{cases} \tag{21}$$

If $\sqrt{(c_{\mathsf{x},k+1} - c_{\mathsf{x},k})^2 + (c_{\mathsf{y},k+1} - c_{\mathsf{y},k})^2} > g$, the segmentation results are ignored, where g is a predefined constant. Subsequently, the sample points were only predicted using the dynamic model, i.e., they were not updated by filter.

In order to find the sequence of corresponding points over time, the *symmetric nearest neighbor correspondences* [24] is applied by sampling a set of equally spaced points along the LV boundary. The construction of a sequence of points is essential to analyze wall motion regionally. Using spline interpolation, N_s points were sampled along the LV cavity in each frame, and N points were chosen as measurements to the filter. A kernel density estimation based on the Gaussian kernel is applied to obtain the probability density. The radial distance for each dataset is normalized with respect to maximum value, allowing analysis of different long-axis segments, namely, apical, mid, and basal, without additional processing.

B. SDE of Normalized Radial Distance

We define the following normalized radial distance r_k^i by

$$r_k^i = \frac{\sqrt{\left(\hat{\mathsf{x}}_k^i - \frac{1}{N}\sum_i \hat{\mathsf{x}}_k^i\right)^2 + \left(\hat{\mathsf{y}}_k^i - \frac{1}{N}\sum_i \hat{\mathsf{y}}_k^i\right)^2}}{\max_i \sqrt{\left(\hat{\mathsf{x}}_k^i - \frac{1}{N}\sum_i \hat{\mathsf{x}}_k^i\right)^2 + \left(\hat{\mathsf{y}}_k^i - \frac{1}{N}\sum_i \hat{\mathsf{y}}_k^i\right)^2}} \tag{22}$$

where $\hat{\mathsf{x}}_k^i$ and $\hat{\mathsf{y}}_k^i$ are the estimates of x_k^i and x_k^i, respectively.

Let $\mathbf{r} \in \mathbb{R}$ be a random variable. The kernel density estimate of the normalized radial distance is given by

$$f(\mathbf{r}) = \frac{\sum_{i,k} \mathcal{K}_\sigma(r_k^i - \mathbf{r})}{N \times K} \tag{23}$$

where

$$\mathcal{K}_\sigma(y) = \frac{1}{\sqrt{2\pi\sigma^2}} \exp\left(-\frac{y^2}{2\sigma^2}\right) \tag{24}$$

is the Gaussian kernel. In this study, the SDE is derived as follows:

$$S_f = -\int_{\mathbf{r}\in\mathbb{R}} \frac{\sum_{i,k} \mathcal{K}_\sigma(r_k^i - \mathbf{r})}{NK} \times \left(\ln \sum_{i,k} \mathcal{K}_\sigma(r_k^i - \mathbf{r}) - \ln NK\right) d\mathbf{r}. \tag{25}$$

We further derive two other information theoretic criteria to measure the *global* information, one is based on the Rényi entropy

$$R_f^\alpha = \frac{1}{1-\alpha} \ln \int_{\mathbf{r}\in\mathbb{R}} \left(\frac{\sum_{i,k} \mathcal{K}_\sigma(r_k^i - \mathbf{r})}{NK}\right)^\alpha d\mathbf{r} \quad \forall\, 0 < \alpha < \infty,\ \alpha \neq 1 \tag{26}$$

and the other on Fisher information

$$I_f = 4 \int_{\mathbf{r}\in\mathbb{R}} |\nabla g(\mathbf{r})|^2 d\mathbf{r} \tag{27}$$

where

$$g(\mathbf{r}) = \sqrt{\frac{\sum_{i,k} \mathcal{K}_\sigma(r_k^i - \mathbf{r})}{NK}}. \tag{28}$$

V. Experiments

The data contain 269 short-axis image datasets, each consisting of 20 functional 2-D images acquired from 20 normal and 10 abnormal hearts. The data were acquired on 1.5T MRI scanners with fast-imaging employing steady-state acquisition (FIESTA) mode. The parameters weighting the relative contribution of the overlap prior, the mean-matching term, and the boundary terms are selected as $\alpha = 1000, \beta = 10, \lambda = 0.1,$ and $c = 10$. The dynamic model and Kalman filter parameters are chosen as $q_1 = 0.2$, $q_2 = 1$, $g = 6$, and $r = 1$ to accommodate noise that account for modeling uncertainties. Please note that choosing noise parameters that misrepresent the modeling uncertainties will degrade the performance of the filtering algorithm. In Fig. 2, we give a representative sample of segmentation results by level set overlap prior method with subsequent Kalman filter smoothing. The second row depicts typical examples, where the method included the papillary muscles inside the target cavity, although these have an intensity profile similar to the surrounding myocardium.

The experiments compare the proposed information theoretic measure based on SDE with other classifier elements, namely, the mean radial displacement and mean systolic radial velocity, as well as other information measures, namely, Rényi entropy ($\alpha = 2$) and Fisher information. Radial velocity computations are based on systolic phase of cardiac cycle. The results were compared with ground truth classification of the cine MRI datasets by experienced medical professionals. A heart is considered to be abnormal in an image dataset if any of its segments [25] is abnormal.

We used two criteria to measure the performance of each classifier element, namely, classification accuracy via

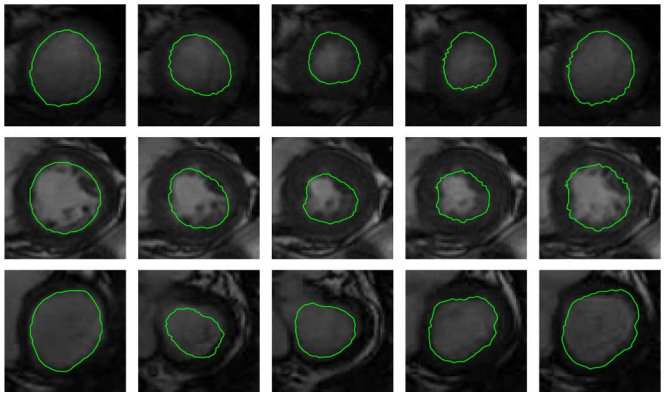

Fig. 2. Representative examples of the LV boundary tracking using level set overlap prior method with subsequent Kalman filtering smoothing: apical (first row), mid-cavity (second row), and basal (third row) frames. The second row depicts typical examples, where the method included the papillary muscles inside the target cavity, although these have an intensity profile similar to the surrounding myocardium.

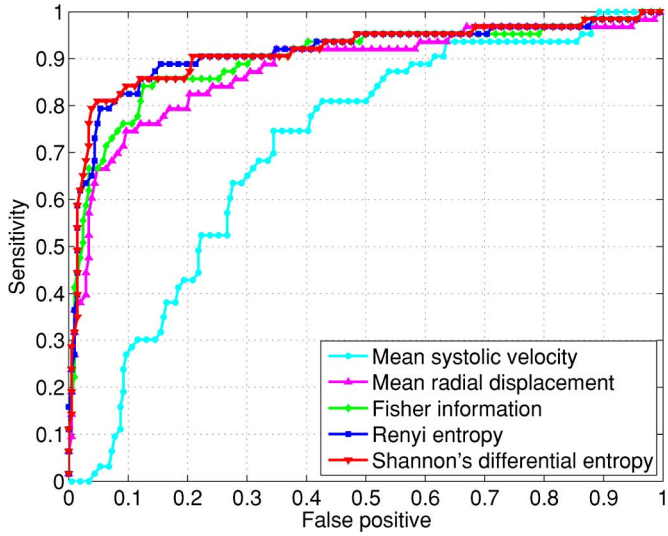

Fig. 3. ROCs of classifier elements. The closer the curve to the left-hand top corner, the better the classification performance. *The proposed information theoretic measure based on the SDE outperforms other classifier elements.*

TABLE I
AUC CORRESPONDING TO FIG. 3 AND BHATTACHARYYA DISTANCE METRIC OF NORMAL/ABNORMAL DISTRIBUTIONS GIVEN IN FIG. 4 FOR CLASSIFIER ELEMENTS

Classifier element	AUC (%)	Bhattacharyya distance metric ($\mathcal{B}$)
Mean systolic velocity	70.8	0.32
Mean radial displacement	87.3	0.53
Fisher information	89.3	0.59
Rényi entropy	90.8	0.60
Shannon's differential entropy	90.9	0.62

TABLE II
PERCENTAGE OF CLASSIFICATION ACCURACY USING LEAVING-ONE-SUBJECT-OUT METHOD FOR CLASSIFIER ELEMENTS

Classifier element	Classification accuracy (%) Abnormal	Normal
Mean systolic velocity	79.4	54.9
Mean radial displacement	76.2	70.9
Fisher information	84.1	85.0
Rényi entropy	87.3	84.5
Shannon's differential entropy	90.5	78.6

leave-one-subject-out method, and the receiver operating characteristic (ROC) curves [26] with corresponding area under the curves (AUCs) [27]. Furthermore, we used the Bhattacharyya measure to assess the discriminative power of each classifier elements. Table I summarizes the results.

A. ROC and AUC

The ROC curves for classifier elements are shown in Fig. 3. The more inclined the curve toward the upper left corner, the better the classifier's ability to discriminate between abnormal and normal hearts. The plot shows that the proposed SDE has superior classifying ability than other classifier elements. The AUCs that correspond to the ROC curves in Fig. 3 are reported in Table I. The AUC represents the average of the classifier sensitivity over false-positive resulting from considering different threshold values, and gives an overall summary of the classification accuracy. The SDE yielded the highest AUC, and therefore, has the best performance.

B. Bhattacharyya Measure

We used the Bhattacharyya distance metric to evaluate the overlap between the distributions of classifier elements over normal and abnormal motions. The Bhattacharyya metric [21] is given by

$$\mathcal{B} = \sqrt{1 - \sum_{y \in \mathbb{R}} \sqrt{f_N(y) f_A(y)}} \tag{29}$$

where f_N and f_A are the distributions over normal and abnormal hearts, respectively. The higher $\mathcal{B}$, the lesser the overlap (Refer to Fig. 4 for an illustration), and therefore, the better the discriminative ability of the classifier. The SDE yielded the highest $\mathcal{B}$, as reported in Table I, and therefore, the best discriminative ability. This is consistent with the previous findings based on ROC/AUC evaluations.

C. Classification Accuracy

Evaluating the percentage of correctly classified hearts using *leaving-one-subject-out* method, the proposed SDE yielded 90.5% sensitivity for a specificity of 78.6%, i.e., 90.5% of abnormal hearts and 78.6% of normal hearts were classified correctly, which is the best overall performance among the reported classifier elements in Table II.

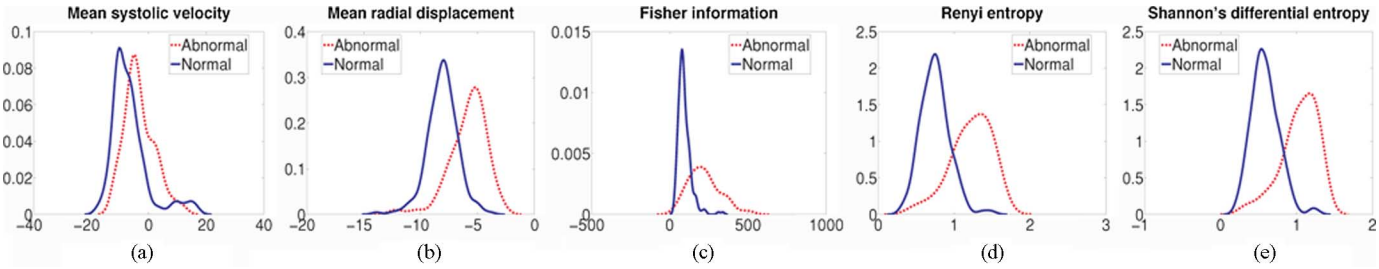

Fig. 4. Distribution of normal and abnormal hearts categorized using classifier elements. *The Bhattacharyya distance metric shows that information theoretic measure based on the SDE has better discriminative ability over other classifier elements*. (a) $\mathcal{B} = 0.32$. (b) $\mathcal{B} = 0.53$. (c) $\mathcal{B} = 0.59$. (d) $\mathcal{B} = 0.60$. (e) $\mathcal{B} = 0.62$.

VI. Conclusion

We derived an information theoretic measure of heart motion based on the SDE, which allows heart wall motion abnormality detection. In the preprocessing step, an overlap prior-based segmentation was used to generate LV contours and the results were subsequently processed using Kalman filter, given a cyclic dynamic model. The proposed method analyzed wall motion quantitatively by constructing distributions of the radial distance estimates of the LV cavity. We further derived two other possible information theoretic abnormality detection criteria, one is based on Rényi entropy and the other on Fisher information. The experimental analysis was performed using 269×20 short-axis MRI obtained from 30 subjects. The results, based on ROCs, AUCs, Bhattacharyya distance metrics, and *leave-one-out* cross validation, showed that the proposed SDE can lead to a significant improvement over other prevalent classifier elements.

Appendix A

Definition of the Curve Evolution Tracking Functional

In this appendix, we give the expression of overlap measure $\mathbf{B}^k$, mean μ^k, and edge-indicator function g_k used in the definition of the tracking functional.

A. Overlap Measure

To define overlap measure $\mathbf{B}^k$, we first consider the following definitions.

1) For each region $\mathbf{R} \in \{C^k, B^k, k \in [1, \ldots, K]\}$, define $P_{\mathbf{R},I}$ as the nonparametric (kernel-based) estimate of intensity distribution within region $\mathbf{R}$ in frame $I \in \{I^k, k \in [1, \ldots, K]\}$

$$\forall z \in \mathbb{R}^+, \quad P_{\mathbf{R},I}(z) = \frac{\int_{\mathbf{R}} K(z - I) d\mathbf{x}}{a_{\mathbf{R}}} \tag{30}$$

where $a_{\mathbf{R}}$ is the area of region $\mathbf{R}$

$$a_{\mathbf{R}} = \int_{\mathbf{R}} d\mathbf{x} \tag{31}$$

Typical choices of K are the Dirac function and the Gaussian kernel given by

$$K(y) = \frac{1}{\sqrt{2\pi h^2}} \exp\left(-\frac{y^2}{2h^2}\right) \tag{32}$$

where h is the kernel width. In this paper, we used the Dirac function, which yields the histogram of intensity within the region.

2) $\mathcal{B}(f/g)$ is the Bhattacharyya coefficient measuring the amount of overlap between two statistical samples f and g

$$\mathcal{B}(f/g) = \sum_{z \in \mathbb{R}^+} \sqrt{f(z)g(z)}. \tag{33}$$

Note that the values of $\mathcal{B}$ are always in $[0, 1]$, where 0 indicates that there is no overlap, and 1 indicates a perfect match.

Assuming the cavity and myocardium regions in the first frame I^1, denoted by C^1 and M, respectively, are given, $\mathbf{B}^k$ measures the overlap between the intensity distribution within the heart cavity in current frame I^k, and the myocardium model distribution learned *a priori* from the first frame

$$\mathbf{B}^k = \mathcal{B}(P_{C^k,I^k}/P_{M,I^1}) \quad \forall k \in [1, \ldots, K]. \tag{34}$$

B. Intensity Mean

Intensity mean of the cavity in current frame I^k is given by

$$\mu^k = \frac{\int_{C^k} I^k d\mathbf{x}}{a_{C^k}}. \tag{35}$$

C. Edge-Indicator Function

The edge-indicator function is given by

$$g_k = \frac{1}{1 + \|\nabla I^k\|^2} \quad \forall k \in [1, \ldots, K] \tag{36}$$

where $\|.\|$ denotes the Euclidean norm.

Appendix B

Discretization of Continuous-Time State-Space Model

The continuous-time state equation (2) has the following solution:

$$\xi(t) = F_{cy}(t, t_0)\xi(t_0) + \int_{t_0}^{t} F_{cy}(t, \tau) B w(\tau) d\tau. \tag{37}$$

The transition matrix has the following properties:

$$\frac{dF_{cy}(t, t_0)}{dt} = A(t) F_{cy}(t, t_0) \tag{38}$$

$$F_{cy}(t_2, t_0) = F_{cy}(t_2, t_1) F_{cy}(t_1, t_0) \qquad \forall t_1 \tag{39}$$

$$F_{cy}(t, t) = I. \tag{40}$$

$$q_{11} = q_1^2 T \tag{56}$$

$$q_{12} = q_{21} = \frac{q_1^2(\omega T - \sin(\omega T))}{\omega} \tag{57}$$

$$q_{13} = q_{31} = q_1^2(1 - \cos(\omega T)) \tag{58}$$

$$q_{22} = \frac{1}{2}\frac{q_1^2\omega^2(3\omega T - 4\sin(\omega T) + \cos(\omega T)\sin(\omega T)) + q_2^2(\omega T - \cos(\omega T)\sin(\omega T))}{\omega^3} \tag{59}$$

$$q_{23} = q_{32} = \frac{1}{2}\frac{q_1^2\omega^2(1 - 2\cos(\omega T) + \cos^2(\omega T)) + q_2^2\sin^2(\omega T)}{\omega^2} \tag{60}$$

$$q_{33} = -\frac{1}{2}\frac{q_1^2\omega^2(\cos(\omega T)\sin(\omega T) - \omega T) - q_2^2(\cos(\omega T)\sin(\omega T) - \omega T)}{\omega} \tag{61}$$

From (39) and (40), we obtain

$$F_{cy}(t, t_0) = F_{cy}(t, t_0)^{-1}. \tag{41}$$

The transition matrix has no explicit form unless it satisfies the following *commutativity property*.

$$A(t)\int_{t_0}^{t} A(\tau)d\tau = \int_{t_0}^{t} A(\tau)d\tau A(t). \tag{42}$$

Then,

$$F_{cy}(t, t_0) = \exp\left(\int_{t_0}^{t} A(\tau)d\tau\right). \tag{43}$$

For a time-invariant system, assuming $t = 0$

$$F_{cy}(t) \stackrel{\triangle}{=} F_{cy}(t, 0) = \exp(At). \tag{44}$$

The transition matrix A of the continuous state-space model (2) is given by

$$A = \begin{bmatrix} 0 & 0 & 0 \\ 0 & 0 & 1 \\ \omega^2 & -\omega^2 & 0 \end{bmatrix}. \tag{45}$$

Evaluating $\exp(At)$ yields

$$\exp(At) = \begin{bmatrix} 1 & 0 & 0 \\ 1 - \cos(\omega t) & \cos(\omega t) & \frac{1}{\omega}\sin(\omega t) \\ \omega\sin(\omega t) & -\omega\sin(\omega t) & \cos(\omega t) \end{bmatrix}. \tag{46}$$

The state at sampling time t_{k+1} can be written as follows:

$$\xi(t_{k+1}) = F_{cy}(t_{k+1}, t_k)\xi(t_k) + w(t_k). \tag{47}$$

For a *time-invariant* continuous-time system, the transition matrix is as follows:

$$F_{cy}(t_{k+1}, t_k) = F_{cy}(t_{k+1} - t_k)$$

$$= \exp((t_{k+1} - t_k)A) \stackrel{\triangle}{=} F_{cy}(k). \tag{48}$$

The discrete-time process noise relates to that of continuous time as follows:

$$w(t_k) = \int_{t_k}^{t_{k+1}} \exp((t_{k+1} - \tau)A)Bw(\tau)d\tau \stackrel{\triangle}{=} w(k). \tag{49}$$

We assume $w(t)$ is zero-mean and white noise. It follows that

$$\mathbb{E}[w(k)] = \mathbf{0}_{2\times 1} \tag{50}$$

$$\mathbb{E}[w(k)w(l)^T] = Q_k\delta_{kl} \tag{51}$$

where δ_{kl} is the Kronecker delta function. The covariance Q_k can be simplified as follows:

$$Q_k = \int_{t_k}^{t_{k+1}} \exp((t_{k+1} - \tau)A)B\Gamma(\tau)B^T \exp((t_{k+1} - \tau)A^T)d\tau \tag{52}$$

where

$$\Gamma(\tau) = \mathbb{E}[w(\tau)w(\tau)^T] \tag{53}$$

$$= \begin{bmatrix} q_1^2 & 0 \\ 0 & q_2^2 \end{bmatrix}. \tag{54}$$

Solving (52) yields

$$Q_k = [q_{ij}]_{3\times 3} \tag{55}$$

where (56)–(61) shown at the top of the page.

References

[1] J. G. Bosch, F. Nijland, S. C. Mitchell, B. P. Lelieveldt, O. Kamp, J. H. Reiber, and M. Sonka, "Computer-aided diagnosis via model-based shape analysis: Automated classification of wall motion abnormalities in echocardiograms," *Acad. Radiol.*, vol. 12, no. 3, pp. 358–367, 2005.

[2] K. Y. Leung and J. G. Bosch, "Localized shape variations for classifying wall motion in echocardiograms," in *Medical Image Computing and Computer-Assisted Intervention 2007*, ser. LNCS, N. Ayache *et al.*, Eds., vol. 4791. New York: Springer-Verlag, 2007, pp. 52–59.

[3] M. Qazi, G. Fung, S. Krishnan, J. Bi, R. B. Rao, and A. Katz, "Automated heart abnormality detection using sparse linear classifiers," *IEEE Eng. Med. Biol. Mag.*, vol. 26, no. 2, pp. 56–63, Mar./Apr. 2007.

[4] Z. Qian, Q. Liu, D. N. Metaxas, and L. Axel, "Identifying regional cardiac abnormalities from myocardial strains using spatio-temporal tensor analysis," in *Medical Image Computing and Computer-Assisted Intervention 2008*, ser. LNCS, D. Metaxas *et al.*, Eds., vol. 5241. New York: Springer-Verlag, 2008, pp. 789–797.

[5] S. Mansor and J. Noble, "Local wall motion classification of stress echocardiography using a hidden markov model approach," in *Proc. 5th IEEE Int. Symp. Biomed. Imag.: Nano Macro*, May 2008, pp. 1295–1298.

[6] A. Suinesiaputra, A. Frangi, T. Kaandorp, H. Lamb, J. Bax, J. Reiber, and B. Lelieveldt, "Automated detection of regional wall motion abnormalities based on a statistical model applied to multislice short-axis cardiac MR images," *IEEE Trans. Med. Imag.*, vol. 28, no. 4, pp. 595–607, Apr. 2009.

[7] I. Ben Ayed, Y. Lu, S. Li, and I. Ross, "Left ventricle tracking using overlap priors," in *Medical Image Computing and Computer-Assisted Intervention 2008*, ser. LNCS, D. Metaxas *et al.*, Eds., vol. 5241. New York: Springer-Verlag, 2008, pp. 1025–1033.

[8] I. Ben Ayed, S. Li, and I. Ross, "Embedding overlap priors in variational left ventricle tracking," *IEEE Trans. Med. Imag.*, vol. 28, no. 12, pp. 1902–1913, Dec. 2009.

[9] I. Ben Ayed, S. Li, and I. Ross, "A statistical overlap prior for variational image segmentation," *Int. J. Comput. Vis.*, vol. 85, no. 1, pp. 115–132, 2009.

[10] Y. Bar-Shalom, X. R. Li, and T. Kirubarajan, *Estimation with Applications to Tracking and Navigation*. New York: Wiley, 2002.
[11] T. M. Cover and J. A. Thomas, *Elements of Information Theory*. New York: Wiley-Interscience, 1991.
[12] R. A. Fisher, "Theory of statistical estimation," *Proc. Cambridge Philos. Soc.*, vol. 22, pp. 700–725, 1925.
[13] B. R. Frieden, *Physics from Fisher Information: A Unification*. Cambridge, U.K.: Cambridge Univ. Press, Jan. 1999.
[14] J. Kim, I. Fisher, J.W., A. Yezzi, M. Cetin, and A. Willsky, "A nonparametric statistical method for image segmentation using information theory and curve evolution," *IEEE Trans. Image Process.*, vol. 14, no. 10, pp. 1486–1502, Oct. 2005.
[15] I. Ben Ayed, S. Li, and I. Ross, "Tracking distributions with an overlap prior," in *Proc. IEEE Conf. Comp. Vis. Pattern Recognit.*, Jun. 2008, pp. 1–7.
[16] E. Biglieri, J. Proakis, and S. Shamai, "Fading channels: Information-theoretic and communications aspects," *IEEE Trans. Inf. Theory*, vol. 44, no. 6, pp. 2619–2692, Oct. 1998.
[17] C. Studholme, D. L. G. Hill, and D. J. Hawkes, "An overlap invariant entropy measure of 3d medical image alignment," *Pattern Recognit.*, vol. 32, no. 1, pp. 71–86, 1999.
[18] Y. M. Zhu, "Volume image registration by cross-entropy optimization," *IEEE Trans. Med. Imag.*, vol. 21, no. 2, pp. 174–180, Feb. 2002.
[19] D. Lake, "Renyi entropy measures of heart rate gaussianity," *IEEE Trans. Biomed. Eng.*, vol. 53, no. 1, pp. 21–27, Jan. 2006.
[20] A. Porta, S. Guzzetti, N. Montano, R. Furlan, M. Pagani, A. Malliani, and S. Cerutti, "Entropy, entropy rate, and pattern classification as tools to typify complexity in short heart period variability series," *IEEE Trans. Biomed. Eng.*, vol. 48, no. 11, pp. 1282–1291, Nov. 2001.
[21] D. Comaniciu, V. Ramesh, and P. Meer, "Kernel-based object tracking," *IEEE Trans. Pattern Anal. Mach. Intell.*, vol. 25, no. 5, pp. 564–577, May 2003.
[22] J. McEachen, A. Nehorai, and J. Duncan, "Multiframe temporal estimation of cardiac nonrigid motion," *IEEE Trans. Image Process.*, vol. 9, no. 4, pp. 651–665, Apr. 2000.
[23] X. Rong Li and V. Jilkov, "Survey of maneuvering target tracking. Part I: Dynamic models," *IEEE Trans. Aerosp. Electron. Syst.*, vol. 39, no. 4, pp. 1333–1364, Oct. 2003.
[24] X. Papademetris, A. Sinusas, D. Dione, R. Constable, and J. Duncan, "Estimation of 3-d left ventricular deformation from medical images using biomechanical models," *IEEE Trans. Med. Imag.*, vol. 21, no. 7, pp. 786–800, Jul. 2002.
[25] M. D. Cerqueira, N. J. Weissman, V. Dilsizian, A. K. Jacobs, S. Kaul, W. K. Laskey, D. J. Pennell, J. A. Rumberger, T. Ryan, and M. S. Verani, "Standardized myocardial segmentation and nomenclature for tomographic imaging of the heart: A statement for healthcare professionals from the cardiac imaging committee of the council on clinical cardiology of the american heart association," *Circulation*, vol. 105, no. 4, pp. 539–542, 2002.
[26] K. H. Zou, J. A. O'Malley, and L. Mauri, "Receiver-operating characteristic analysis for evaluating diagnostic tests and predictive models," *Circulation*, vol. 115, no. 5, pp. 654–657, 2007.
[27] J. Hanley and B. McNeil, "The meaning and use of the area under a receiver operating characteristic (roc) curve," *Radiology*, vol. 143, no. 1, pp. 29–36, 1982.

Kumaradevan Punithakumar received the B.Sc. Eng. (with First class Hons.) degree in electronic and telecommunication engineering from the University of Moratuwa, Moratuwa, Sri Lanka, in 2001, and the M.A.Sc. and Ph.D. degrees in electrical and computer engineering from McMaster University, Hamilton, ON, Canada, in 2003 and 2007, respectively.

From 2002 to 2007, he was a Teaching Assistant in Electrical and Computer Engineering Department, McMaster University, where he became a Postdoctoral Research Fellow in 2008. He is currently an Associate Imaging Research Scientist at GE Healthcare, London, ON, Canada. His research interests include medical image analysis, target tracking, sensor management, and computer vision.

Dr. Punithakumar was the recipient of the Industrial R&D Fellowship by the National Sciences and Engineering Research Council of Canada in 2008.

Ismail Ben Ayed received the Ph.D. degree in computer science from the Institut National de la Recherche Scientifique, Montreal, QC, Canada.

He is currently a Scientist with GE Healthcare, London, ON, Canada. His research interests include computer vision, pattern recognition, and medical image analysis.

Ian G. Ross received the M.D. degree from Queen's University, Kingston, ON, Canada.

He was with Kingston General Hospital, Queen's University for residency training in diagnostic radiology. He was a Clinical Fellow in body musculoskeletal imaging at the University of Western Ontario, London, ON for one year. In 2005, he joined as an Assistant Professor of radiology at the University of Western as well as a Staff Radiologist at University Hospital, and since then, he has been performing cross-sectional imaging with a special interest in cardiac computed tomography. He is currently the Medical Leader in general radiology and sports medicine with London Health Science Center, London, ON, where he is engaged with the research.

Ali Islam received the B.Sc. degree from the University of Ottawa, Ottawa, ON, Canada and the M.D. degree from the University of Toronto, Toronto, ON, in 1995 and 1999, respectively.

In 2004, he was with the University of Western Ontario, London, ON for residency training in diagnostic radiology. He was a Clinical Fellow in cardiovascular imaging with the Cleveland Clinic, Cleveland, OH, in 2005. He is currently practicing and teaching radiology at St. Joseph's Health Care, London, ON. He is also the Co-Director of the cardiovascular imaging computed tomography and MRI Fellow at the Schulich School of Medicine, University of Western Ontario. His research interests include segmentation of cardiac images and developing novel collaboration and communications tools for picture archiving and communication system.

Jaron Chong received the B.H.Sc. degree from McMaster University, Hamilton, ON, Canada and the M.D. degree from the University of Western Ontario, London, ON. He is currently working toward a medical residency in diagnostic radiology at McGill University, Montreal, QC, Canada.

Shuo Li received the Ph.D. degree from the Department of Computer Science and Software Engineering, Concordia University, Montreal, QC, Canada, in 2006.

He is currently a Research Scientist and a Project Manager in GE Healthcare, London, ON, Canada. He is also an Adjunct Research Professor in the Department of Medical Biophysics and Medical Imaging, University of Western Ontario, London, ON. He is the Head of the Digital Imaging Group of London (http://dig.lhsc.on.ca/). His research interests include the computer-automated medical image analysis and visualization.